

4

AD-A220 859

GL-TR-89-0233
ENVIRONMENTAL RESEARCH PAPERS, NO. 1048

**The Importance of Adiabatic Variations in Trapped Particle
Distributions Observed by the SCATHA Satellite**

J.N. BASS
M.S. GUSSENHOVEN
R.H. REDUS



29 November 1989

DTIC
ELECTE
APR 24 1990
S B D
Co



Approved for public release; distribution unlimited.



SPACE PHYSICS DIVISION

PROJECT 7601

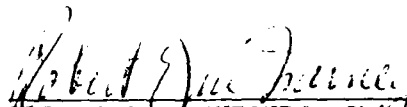
GEOPHYSICS LABORATORY

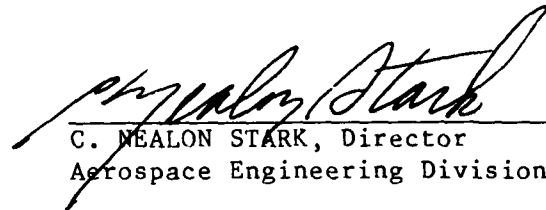
HANSCOM AFB, MA 01731-5000

90 04 23 041

"This technical report has been reviewed and is approved for publication"

FOR THE COMMANDER


ROBERT E. MCINERNEY, Chief
Data Systems Branch
Aerospace Engineering Division


C. NEALON STARK, Director
Aerospace Engineering Division

This report has been reviewed by the ESD Public Affairs Office (PA) and is releasable to the National Technical Information Service (NTIS).

Qualified requestors may obtain additional copies from the Defense Technical Information Center. All others should apply to the National Technical Information Service.

If your address has changed, or if you wish to be removed from the mailing list, or if the addressee is no longer employed by your organization, please notify GL/IMA, Hanscom AFB, MA 01731. This will assist us in maintaining a current mailing list.

Do not return copies of this report unless contractual obligations or notices on a specific document requires that it be returned.

REPORT DOCUMENTATION PAGE

1a. REPORT SECURITY CLASSIFICATION Unclassified		1b. RESTRICTIVE MARKINGS	
2a. SECURITY CLASSIFICATION AUTHORITY		3. DISTRIBUTION / AVAILABILITY OF REPORT Approved for Public Release Distribution Unlimited	
2b. DECLASSIFICATION / DOWNGRADING SCHEDULE		5. MONITORING ORGANIZATION REPORT NUMBER(S)	
4. PERFORMING ORGANIZATION REPORT NUMBER(S) GL-TR-89-0233 ERP, No. 1048		5. MONITORING ORGANIZATION REPORT NUMBER(S)	
6a. NAME OF PERFORMING ORGANIZATION Geophysics Laboratory	6b. OFFICE SYMBOL (if applicable) PHP	7a. NAME OF MONITORING ORGANIZATION	
6c. ADDRESS (City, State, and ZIP Code) Hanscom AFB Massachusetts 01731-5000		7b. ADDRESS (City, State, and ZIP Code)	
8a. NAME OF FUNDING / SPONSORING ORGANIZATION	8b. OFFICE SYMBOL (if applicable)	9. PROCUREMENT INSTRUMENT IDENTIFICATION NUMBER	
8c. ADDRESS (City, State, and ZIP Code)		10. SOURCE OF FUNDING NUMBERS	
		PROGRAM ELEMENT NO. 62101F	PROJECT NO. 7601
		TASK NO. 22	WORK UNIT ACCESSION NO. 01
11. TITLE (Include Security Classification) The Importance of Adiabatic Variations in Trapped Particle Distributions Observed by the SCATHA Satellite			
12. PERSONAL AUTHOR(S) J. N. Bass*, M. S. Gussenhoven, R. H. Redus			
13a. TYPE OF REPORT Scientific Interim	13b. TIME COVERED FROM 3/87 TO 2/89	14. DATE OF REPORT (Year, Month, Day) 1989 November 29	15. PAGE COUNT 38
16. SUPPLEMENTARY NOTATION *Radex, Inc., Bedford, MA			
17. COSATI CODES		18. SUBJECT TERMS (Continue on reverse if necessary and identify by block number)	
FIELD	GROUP	SUB-GROUP	
		Adiabatic variations, Trapped particles, SCATHA, Outer radiation belts, Magnetic field, Mead model, Adiabatic invariants, L-shell	
19. ABSTRACT (Continue on reverse if necessary and identify by block number)			
<p>Fluxes of trapped 20 keV-1 MeV electrons and ions observed by SCATHA from 5 to 8 R_E are analyzed for a magnetically quiet and subsequent disturbed period to determine the contribution adiabatic variations make to the observed large variations. The magnetic field is modeled by a dipole distorted by the sum of an azimuthally symmetric and an asymmetric perturbation, which perturbations are empirically determined functions of time. Distribution functions for the disturbed period are predicted from those observed in the quiet period, assuming conservation of the three adiabatic invariants for magnetically trapped particles. The disturbance discussed here is observed during the ascending portion of the SCATHA orbit, when the satellite climbs from $L=6.2R_E$ to $L=8.2R_E$, and traverses in local time from late afternoon to early morning. The disturbance is first encountered when SCATHA crosses $L=6.2R_E$, $MLT=2140$. It is characterized by a systematic weakening in the plasma sheet magnetic field and concurrent dropouts in the 90° pitch angle high energy electron and ion fluxes. The electron fluxes and the magnetic field remain low for the remainder of this ascending leg, but the ion fluxes recover somewhat for $L>7R_E$. The IMF B_z is small but steadily northward for over</p> <p style="text-align: right;">(OVER)</p>			
20. DISTRIBUTION / AVAILABILITY OF ABSTRACT <input checked="" type="checkbox"/> UNCLASSIFIED/UNLIMITED <input type="checkbox"/> SAME AS RPT <input type="checkbox"/> DTIC USERS		21. ABSTRACT SECURITY CLASSIFICATION Unclassified	
22a. NAME OF RESPONSIBLE INDIVIDUAL M. S. Gussenhoven		22b. TELEPHONE (Include Area Code) (617)377-3212	22c. OFFICE SYMBOL GLPH

Abstract Continued:

24 hours preceding this period, then it turns sharply southward just as SCATHA begins the ascending leg in question, and remains southward until the satellite crosses $L=7.2R_E$. The other two components of the IMF indicate a sector change just after this period. The solar wind velocity decreases at a slow rate before and during this period, while the solar wind ion density is steadily increasing. The AE index, after over 24 hours at very quiet levels, increases rapidly to 360 while the IMF B_z is southward, then recovers after B_z reverses to the north. For magnetic field decompression, such as that observed here, the theory based on conservation of the adiabatic invariants predicts deceleration of equatorially mirroring particles, causing reduction in the fluxes observed at a given energy similar to those seen in the early phase of this event. Therefore one should consider such adiabatic responses to magnetic field variations, along with sources and sinks, in modeling variations in magnetospherically trapped particle fluxes.

ACKNOWLEDGEMENTS

Reduction of SCATHA particle and magnetic field data was performed by D. E. Delorey of Boston College. N. Bonito of Radex, Inc., provided valuable assistance in production of the color figures. Software for the statistical processing of the SCATHA magnetometer data was produced by K. G. Cottrell, formerly of Radex, Inc.

Accession For	
NTIS GRA&I	<input checked="" type="checkbox"/>
DTIC TAB	<input type="checkbox"/>
Unannounced	<input type="checkbox"/>
Justification	
By _____	
Distribution/	
Availability Codes	
Dist	Avail and/or Special
A-1	

CONTENTS

1. INTRODUCTION	1
2. PROCEDURE	2
3. RESULTS	13
4. DISCUSSION	21
REFERENCES	26
APPENDIX	29

ILLUSTRATIONS

1. The Original Mead model, Tsyganenko- Usmanov model, and adjusted Mead model	7
2. Model and measured magnetic fields; electron distribution functions	15
3. The magnetic field observed by SCATHA and computed using an adjusted Mead model	16
4. Comparison of measured and fit distribution function values for 275 keV	18
5. Same as Figure 4, but for 218 keV electrons	19
6. Noon anisotropies	20
7. Adjusted Mead model magnetic field parameters	22
8. Comparison of SCATHA observations of 275 keV ions with predictions based on adiabatic variations from the previous day	23
9. Same as Figure 8, but for 218 keV electrons	24
A1. Equatorial maps of energy density and average energy in a Mead field deduced by adiabatic variation for electrons	31
A2. Anisotropy index for 270 keV electrons	32

TABLES

A1. Parametric Values for Initial Electron Distribution	30
---	----

1. INTRODUCTION

Observations of high energy trapped radiation belt particles at fixed energies, pitch angles, and locations reveal frequent, large variations in number flux (order of magnitude). During storms, significant enhancements of particle populations are often seen which may be associated with injections of new particles into the radiation belts [Williams, Arens, and Lanzerotti, 1968; Paulikas and Blake, 1970]. During geomagnetically quiet times, on the other hand, these populations are observed to slowly decay due to loss processes such as pitch angle diffusion and interaction with the atmosphere [Schultz and Lanzerotti, 1974; Roberts, 1969; Walt, 1966]. Another cause of observed variations at fixed energy, pitch angle, and location is the adiabatic response of particles already trapped in the radiation belts to variations in the magnetic field [Soraas, and Davis, 1968]. In this process particles don't actually leave or enter the radiation belts, but simply change their observable parameters, such as energy, so that their adiabatic invariants are conserved. This changes the identity and number of particles seen in a given energy channel at a given location and position.

Therefore, in the analysis of the dynamics of magnetospherically trapped particle distributions it is necessary to distinguish variations caused by true injections into, and depletions from, the radiation belts, from variations caused by responses of the resident particles to variations in the magnetic field. If the field is sufficiently slowly varying, these responses are determined by the conservation of the three adiabatic invariants. The adiabatic invariants, and the equations representing their conservation, depend on specification of a time-varying magnetic field. From this it follows that the adiabatic behavior of a class of trapped particles could be used as a monitor to classify magnetic field variations. The uniqueness of the classification remains an open question.

This report describes part of an effort to develop new techniques for the analysis of in-situ radiation belt particle data and the remote sensing of time varying magnetic fields. These techniques would utilize ordered relationships between magnetic field and particle data, arising in part from adiabatic motions of the particles in time-varying fields, to deduce global magnetic field variations from locally sensed particle variations. Real-time applications of the techniques would require accurate, but practically applicable techniques for ordering the particle data by magnetic field variations. An approach is described for calculating adiabatic invariants and deriving changes in the particle distribution functions, under the condition that the adiabatic invariants are conserved in the presence of a simple time-varying model magnetic field. This approach uses first order perturbation theory developed by Pennington [1961] and Stern [1965, 1968] for distorted dipole fields. The method derives its efficiency from the use of analytic expressions for magnetic field lines to eliminate the requirement of tracing. This method is applied here to a time-dependent model similar in mathematical form to the Mead [1964] model, but with parameters adjusted to fit magnetometer observations, rather than determined as

(Received for publication 7 November 1989)

specified by Mead to represent magnetopause effects only. As suggested by Luhmann and Schulz [1979], this adjustment permits one to account in an approximate way for the effects of other external sources.

A two day period of SCATHA magnetometer and particle observations has been chosen for this study. The first day is exceptionally quiet, thus serving as a baseline for quiet magnetic field and particle distribution models. Using a quiet magnetic field model and the measured particle distributions along the SCATHA orbit, and assuming conservation of the adiabatic invariants, the quiet time particle distribution functions can be extrapolated to a larger annulus in the equatorial plane. On the second day, a moderately disturbed day, a time-varying magnetic field model is constructed from the magnetometer data. The disturbed magnetic field model together with the quiet day particle distributions and magnetic field model are used, assuming conservation of the adiabatic invariants, to calculate the particle distribution functions for the second day. Comparisons with the observed particle distribution functions for the second day indicate that much of the variations can be attributed to adiabatic response to the magnetic decompression that occurred. Pronounced butterfly distributions observed in the midnight sector concurrent with this decompression are in agreement with the adiabatic calculations. This result suggests that particles might be used as remote sensors of long-term global magnetic field variations. If we can identify classes of particles, by species and energy range, which are found to behave predominantly adiabatically, we can turn the above process around and use their variations to infer global changes in the magnetic field. This would be an important aid in real-time analysis if standard global indices, such as solar wind parameters, are not available.

Previous authors [*Soraas and Davis, 1968; Lyons and Williams, 1976; Lyons, 1977; Lin, Parks, and Winckler, 1976; Kaye, Lin, Parks, and Winckler, 1978*] have also studied adiabatic variations, and obtained similar results. Their work considered only the conservation of the first two adiabatic invariants, or the conservation of all three in an azimuthally symmetric field. These limitations are valid for magnetic field changes on time scales small compared to the particle drift periods, or for small radial distances such that the magnetic field asymmetry can be neglected. One or both of these conditions was satisfied in the cases discussed by these authors. Our effort considers slow time variations of an azimuthally-varying field, and therefore requires incorporation of conservation of the third adiabatic invariant in a non-trivial way. This is necessary to adequately include time variations in the drift shell splitting, which are expected to have an increasing impact on pitch angle distributions with increasing distances.

2. PROCEDURE

In the guiding center approximation, the motion of a magnetospherically trapped particle is resolved into the gyration of the particle about a guiding center, the bounce motion of the guiding center along field lines, and the azimuthal drift motion

of the guiding center across field lines. This approximation is valid so long as the gyration period is much smaller than the bounce period, which in turn is much smaller than the drift period [Schulz and Lanzerotti, 1974]. Associated with each of the three motions is an action integral that is approximately conserved provided the forces on the particle do not vary appreciably over a single cycle of the motion. These action integrals are collectively referred to as the adiabatic invariants. The first adiabatic invariant, associated with the gyration of the particle about its guiding center, is proportional to its magnetic moment,

$$\mu = \frac{p^2 \sin^2 \alpha}{2mB}, \quad (1)$$

where p is the particle's momentum, α is the pitch angle, (the angle between the momentum vector and the magnetic field vector), m is the particle's rest mass, and B is the magnitude of the magnetic field intensity. From the conservation of μ , we can infer that the particle bounces along the field line between two points, called mirror points, which satisfy

$$B = B_m = \frac{B_i}{\sin^2 \alpha_i}, \quad (2)$$

where B_i and α_i are the initial magnetic field intensity magnitude and pitch angle. The second adiabatic invariant,

$$J = 2pl = 2p \int \sqrt{1 - \frac{B}{B_m}} ds, \quad (3)$$

where the integration is along the field line between the two mirror points, allows us to define the drift shell of the particle as that which contains the set of field lines possessing the points with specified B_m and I .

We thus see that in a stationary field we may determine, from a particle's initial position, momentum (or energy), and pitch angle, its first two adiabatic invariants, from which we can in turn determine the trajectory of its guiding center. From Liouville's Theorem, that the distribution function of the particles is conserved over a trajectory, it follows that when we measure the distribution function of a set of particles at a given point, we are also measuring the distribution function at other points in the same particle trajectory. Thus, for example, we learn something about the distribution function at local noon on the equator, even though we are actually observing directly somewhere else. In this way we may summarize the data collected in one orbital pass by a satellite such as SCATHA with a distribution function at the equator at local noon, as was done by Luhmann and Schulz [1979] for the ATS-1 satellite. From this noon equatorial distribution function we may

then calculate distribution functions for the observed particles at all points on their trajectories, not just at points on the satellite's orbit.

For time-varying fields, the above statements are no longer all valid. However, for fields varying slowly on the time scale of one drift period, we may invoke conservation of the third adiabatic invariant, which is proportional to the magnetic flux enclosed by the drift orbit. Then the particle drift orbits may be thought of as slowly varying in time so as to conserve all three adiabatic invariants. This requires time variations in p , B_m , and I , but Liouville's Theorem remains intact. Then, if we have obtained the local noon equatorial distribution functions for a magnetically stationary period, as described above, we can also calculate them for the same particles for the time varying field, albeit that the particles will possess different energies and trajectories. Working backwards, we can calculate distribution functions at specified positions, energies, and pitch angles in a time varying field from the distribution functions at equivalent noon equatorial energies, pitch angles and positions in the stationary field.

In this report, we therefore test the adiabatic theory by first deriving, for a stationary magnetic field, the equatorial noon distribution functions for ions and electrons observed in one orbital pass by the SCATHA satellite. The magnetometer readings during this pass are used to derive a reference Mead-type field, which is used to derive the particle drift shells according to the Pennington-Stern equations. Then for particles observed in a subsequent disturbed field, we transform the energies, pitch angles, and positions to equivalent noon equatorial variables in the reference field, assuming conservation of the three adiabatic invariants. The disturbed field is defined by time-varying Mead parameters derived from the magnetometer data. Given the distribution functions for the equivalent variables in the reference field, the distribution functions for the observed variables in the disturbed field are derived via Liouville's Theorem. These are then compared directly with the observed distribution functions.

2.1 The Magnetic Field Model

The geosynchronous region, $r \approx 6.6R_E$ (where R_E is one Earth radius), may often be considered a current-free region. During magnetically quiet periods, the ring current exerts negligible influence on the radiation belts [Schulz and Lanzerotti, 1974]; storm-time enhancements seem to be confined primarily to the interior [Frank, 1967], except during particle injections in the initial phase of a storm [Lui, et. al., 1987]. Magnetopause currents are, of course, located well to the exterior, as are most of the tail currents, although the Tsyganenko-Usmanov [1982] model indicates storm-time penetration of the inner edge of the tail current system to within $5R_E$.

In a current-free region, the magnetic field may be written as

$$B = -\nabla V_m, \quad (4)$$

where, since B is divergence-less, the potential V_m is a solution of Laplace's equation, with the general form [Chapman and Bartels, 1940]:

$$V_m = \sum_{n=1}^N \sum_{m=0}^n \left(\frac{1}{r}\right)^{n+1} P_n^m(\cos \theta) (g_n^m \cos m\lambda + h_n^m \sin m\lambda) + \sum_{n=1}^{N'} \sum_{m=0}^n r^n P_n^m(\cos \theta) (\bar{g}_n^m \cos mt + \bar{h}_n^m \sin mt), \quad (5)$$

where

r = radial distance, in R_E ,

P_n^m = Associated Legendre Functions, Schmidt normalized [Chapman and Bartels, 1940],

θ = geomagnetic colatitude,

λ = geomagnetic longitude,

t = geomagnetic local time (midnight = 0°).

The first summation contains the contributions due to sources radially interior to the point in question. These include the earth's interior core, which is responsible for what is commonly called the "main" field, and the ring current, if it is sufficiently compressed. Although this portion is usually written in geographic coordinates, we express it here in geomagnetic coordinates (z axis parallel to the dipole) for convenience to the application to be discussed in this paper.

The second summation includes contributions from sources radially exterior to the point in question. These would include the magnetopause and tail currents.

The simplest form of this potential incorporating basic features of the outer radiation belt field is:

$$V_m = \frac{-B_0 \cos \theta}{r^2} - B_1 r \cos \theta + B_2 r^2 \sin \theta \cos \theta \cos(t - \phi), \quad (6)$$

where:

$$B_0 = -g_1^0,$$

$$B_1 = -\bar{g}_1^0,$$

$$B_2 = \sqrt{3[(\bar{g}_2^1)^2 + (\bar{h}_2^1)^2]},$$

$$\cos \phi = \sqrt{3} \frac{\bar{g}_2^1}{B_2},$$

$$\sin \phi = \sqrt{3} \frac{\bar{h}_2^1}{B_2}.$$

The first term is, of course, the geomagnetic dipole term. The other two terms are the first two exterior terms for a field symmetric about the dipole equator, with a local time variation symmetric about the ϕ meridian. For $\phi = 0$ (field symmetric about the noon-midnight meridian), this was the form justifiably chosen by Mead [1964] for representation of the contribution of magnetopause currents to the geomagnetic field. By adjustment of the parameters B_1 , B_2 , and ϕ , in response to observations, we hope to realistically simulate effects of the other important magnetospheric current systems.

The model might of course be improved by the use of additional terms. For instance, exterior terms with $(n + m + 1)$ odd could be added for a field not symmetric about the dipole equator, as is the case when the dipole tilt is non-zero. As mentioned previously, additional interior terms could be used to simulate the effects of a spatially compressed ring current. The Pennington-Stern formulation, described below for the adiabatic motions of the trapped particles, easily accommodates such generalizations, whereas there is no easy analytical procedure available for the familiar magnetospheric models such as the Tsyganenko-Usmanov [1982] and Olson-Pfitzer [1974, 1977] models.

In the equatorial plane the deviation of our simple model from a dipole field is:

$$\Delta B = B_1 - B_2 r \cos(t - \phi). \quad (7)$$

Fig. 1 shows a comparison of ΔB along the earth-sun line, under geomagnetically quiet conditions, for a characteristic version of our model, the Tsyganenko-Usmanov [1982] model, and the original Mead [1964] model. The parameters chosen for our model (the adjusted Mead model) are:

$$B_1 = -10nT,$$

$$B_2 = 3.4nT,$$

$$\phi = 0.$$

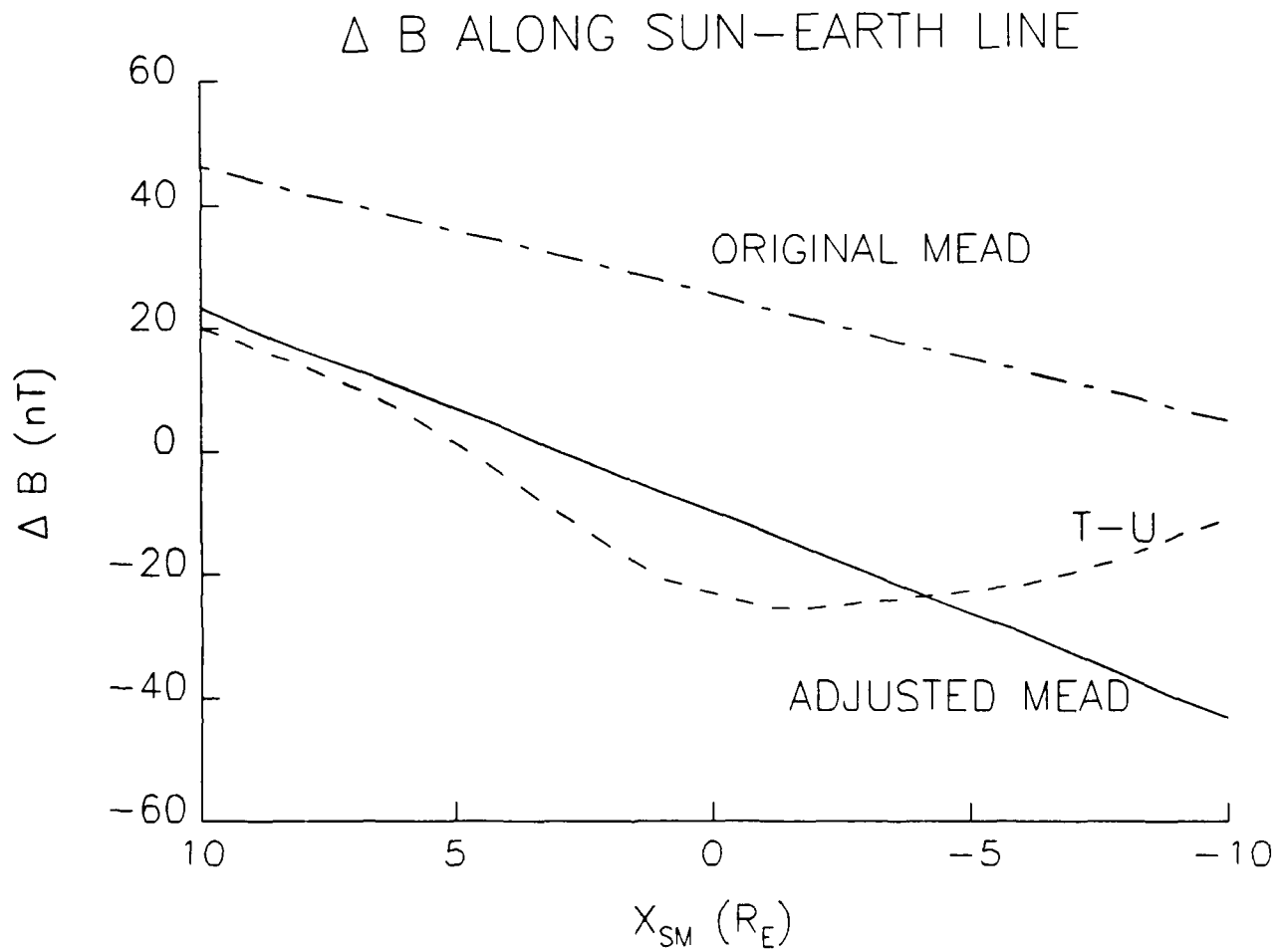


Figure 1. The Original Mead model (stand-off distance = $10R_E$); the $K_p = 0+$ Tsyganenko- Usmanov model for 20 April 1979, 1200 UT; and an adjusted Mead model with $B_1 = -10nT$ and $B_2 = 3.4nT$, are used to calculate the variation from the dipole field, ΔB , which is plotted as a function of distance (in R_E) from the Earth along the Earth-Sun line (positive values toward the Sun).

The Tsyganenko-Uzmanov model is plotted for conditions corresponding to 20 April 1979, 1200 UT, $K_p = 0+$. The original Mead model is for $10R_E$ noon magnetopause stand-off distance. We see that the adjusted simple model roughly simulates the variation of the more dynamic Tsyganenko-Uzmanov model, but that it lacks the near-earth detailed structure of the ring current, and the proper asymptotic behavior at large distances on the night-side.

2.2 Pennington-Stern Equations

The Pennington-Stern equation for the equatorial crossing of a drift shell in a Mead field, such as the one just described, is

$$r_e = L \left(1 - \epsilon_1 \frac{B_1 L^3}{b_0} - \epsilon_2 \frac{B_2 L^4 \cos[t - \phi]}{B_0} \right), \quad (8)$$

where

$L =$ McIlwain [1961] parameter at the mirror points;

$$\epsilon_1 = \bar{\alpha}_1^0;$$

$$\epsilon_2 = -\sqrt{3}\bar{\alpha}_2^1.$$

The $\bar{\alpha}_i^j$ are the same as the α_i^j defined by Pennington [1961] except that $(-n)$ is replaced in all equations by $(n + 1)$ (see Stern [1968]). This reflects the fact that Pennington's original development was for the internal multipoles of the field, which contain terms in r^{-n-1} , while the present development involves external multipoles, containing r^n . These coefficients depend explicitly on the effective dipole mirror point colatitude θ_m , which is related to the equatorial pitch angle α_e by

$$\sin \alpha_e = \frac{\sin^3 \theta_m}{(1 + 3 \cos^2 \theta_m)^{1/4}}. \quad (9)$$

The L value is obtained by solving the drift shell equation to first order in the Mead perturbation parameters B_1 and B_2 [Stern, 1965]:

$$L = r_e \left(1 + \frac{\epsilon_1 B_1 r_e^3}{B_0} + \frac{\epsilon_2 B_2 r_e^4 \cos[t - \phi]}{B_0} \right). \quad (10)$$

The first and second invariants are, from Eqs. (1) and (3):

$$\mu = \frac{p^2}{2mB_m};$$

$$J = 2pI$$

where p is the particle momentum, B_m is the magnetic field value at the particle's mirror points, and I is the familiar longitudinal invariant integral between the mirror points. Schulz and Lanzerotti [1974], p. 17-20, give approximate expressions for I , given B_m and L (these are valid for any field, not just dipole):

$$I = LY = L\{2(1-y)T(0) + [T(0) - T(1)](y \ln y + 2y - 2y^{1/2})\}, \quad (11)$$

where

$$y = \sqrt{\frac{B_0}{B_m L^3}};$$

$$T(0) = 1.3802;$$

$$T(1) = 0.7405.$$

The third invariant, to first order in the Mead perturbation parameters, is computed as:

$$F = \left(-\frac{2\pi B_0}{L}\right) \left[1 + \frac{(\epsilon_1 - 1/2)B_1 L^3}{B_0}\right]. \quad (12)$$

2.3 Determination of Reference Drift Orbits

The three adiabatic invariant conditions are solved to determine the L values, mirror-point magnetic inductions, and momenta in the reference magnetic field, given these values for the disturbed field. The L values are determined first by linearizing the third invariant in L :

$$\Delta L = \frac{-\Delta F}{(\delta F/\delta L)}, \quad (13)$$

where ΔL is the change in L (reference-disturbed), ΔF is the corresponding change in F , for fixed L , and the partial of F with respect to L (in the parentheses) is taken in a fixed dipole field (neglecting the Mead perturbations):

$$\frac{\delta F}{\delta L} = \frac{2\pi B_0}{L^2}. \quad (14)$$

This forms an initial guess for a Newton-Raphson procedure to obtain the exact solution accounting for the nonlinearity of the third adiabatic invariant in L .

The conditions for the first two adiabatic invariants are then solved for the momenta p and mirror-point magnetic inductions B_m in the reference field, after substitution of the L values just obtained for the reference field. These equations reduce to:

$$\sqrt{B_m} I(L, B_m) = \text{constant}. \quad (15)$$

This is solved for B_m by the Newton-Raphson method, using as the initial guess:

$$B_m = \frac{B_d L_d^3}{L^3}, \quad (16)$$

where the subscript d designates the disturbed field. The particle momentum (and thus energy) is then easily obtained by substitution of the resulting solution for B_m into the equation for the first adiabatic invariant.

2.4 Noon Parameters

The noon equatorial crossing is computed directly from the Pennington-Stern drift shell equation, substituting $t = \pi$, and using the reference value of L . The reference Mead induction B_e at this equator crossing is then computed, and used to define the equatorial L value in the reference field:

$$L_e = \left(\frac{B_0}{B_e}\right)^{1/3}. \quad (17)$$

For the equatorially mirroring particles this would be exactly equal to L if the method were exact. The difference

$$\Delta L = L - L_e, \quad (18)$$

for the equatorially mirroring particles, is added to L_e for the particles for all pitch angles, as a sort of "second order" correction. For the low-latitude mirroring particles, this correction is probably very accurate—indeed for the equatorially mirroring particles it is exact. For the high-latitude particles (low pitch angles), a comparison

of the perturbation method with numerical tracing calculations indicates that the error in this correction never exceeds $0.05R_E$ at noon for the reference model used in this report. The revised L_e value then determines a revised B_e value:

$$B_e = \frac{B_0}{L_e^3}, \quad (19)$$

from which the equatorial pitch angle in the reference field is computed as:

$$\alpha_e = \sin^{-1} \sqrt{\frac{B_e}{B_m}}. \quad (20)$$

If the argument of the inverse sine exceeds one, as may result due to the approximations made, it is set to one to avoid an undefined condition. This difficulty only occurs for particles mirroring near the equator, but not, however, for particles mirroring exactly on the equator, since these maintain their precisely 90° pitch angles. The L_e correction procedure described above alleviates this situation somewhat, since the equatorial crossing fields B_e of the low-latitude mirroring particles are more accurately determined.

2.5 Quiet Modelling

The SCATHA magnetometer and particle data for a quiet day are analyzed to provide two inputs required for the prediction of the disturbed particle distributions: the reference magnetic field and particle models.

The reference magnetic field is determined by fitting the magnetometer data for a quiet day (one full SCATHA orbit) to a Mead-type (three parameter) model as specified above. We emphasize that this resulting model therefore is not identical to the original Mead model, which incorporates only magnetopause surface currents to augment the central dipole; rather, as suggested by Luhmann and Schulz [1979], the fit attempts to empirically simulate the real effects of ring and surface currents as well. In contrast to those authors, we have used all the data for a quiet day, rather than just the local noon and midnight magnetometer readings, and we have allowed the local time symmetry axis to differ from the traditionally assumed noon-midnight meridian. Other authors [Cummings, Coleman, and Siscoe, 1971; Pfitzer, Lezniak, and Winckler, 1969] have observed such a rotation.

The reference (quiet time) particle model, which is used as an input in predicting the disturbed period particle observations, must describe the particle distributions at all local times and throughout the L range covered by SCATHA, yet it must be developed from a single SCATHA orbit (i. e., a limited combination of local time and L). To do this, we follow the method of Luhmann and Schulz [1979], mapping

the particle distributions from the points of observations to local noon, assuming the conservation of adiabatic invariants and the magnetic field model described above. Then at local noon we attempt to fit the mapped observations to the product of two functions: one representing the L dependence of the particles with 90° pitch angles and the other an L -dependent pitch angle distribution. At local noon, we have (for energy E)

$$F(\alpha_e, L_e, E) = f(\alpha_e, L_e, E)g(L_e, E), \quad (21)$$

where g is the distribution of the 90° particles and f is the pitch angle distribution, normalized to unity at 90° . The function g has been found to decrease exponentially with L_e (although piece-wise exponential fits were required for the electrons), while f was described by a linear combination of the first two orthonormal basis functions of Schulz and Boucher [1984, Eq. 14], which are eigenfunctions of a simple pitch angle diffusion operator. It was found that the coefficients for the functional dependence of f had to be made weakly dependent on L_e to normalize the distributions to unity at 90° and to reproduce the observed ratio $F(45)/F(90)$. Given this distribution at local noon, we can then map the particles to any point in the observation space using the techniques described above.

2.6 Disturbed Magnetic Field Modelling

The magnetometer data for the disturbed period are fit to the same Mead-type model as the quiet-time data, except that the coefficients are now time-dependent, and we fit them to piecewise continuous functions. The resulting magnetic model is combined with the reference magnetic field and particle models described above to predict the disturbed particle distributions that should be observed by SCATHA from the adiabatic theory described previously.

2.7 Illustration

In the appendix we illustrate an application of this procedure to a group of test particles initially distributed uniformly in a circular ring 6.5 to 7.0 R_E in a dipole field. They are also uniformly distributed in a narrow energy range 300-400 keV, with a normal pitch angle distribution (peaked at 90°). We see that, for a typically asymmetric deformation of the field (more compressed on the day side, decompressed on the night side), with an average overall decompression, the test particles with 90° pitch angles undergo a substantial deceleration (loss of energy), and that butterfly pitch angle distributions form at certain locations.

3. RESULTS

3.1 SCATHA Orbit and Instrumentation

The P78-2 SCATHA satellite was launched on January 30, 1979. Seventy-two hours after launch, the satellite was inserted into a $5.3R_E \times 7.8R_E$, low-inclination (7.9°) orbit with an easterly drift rate of about 5° per day. The satellite is spin stabilized at approximately 1 rpm, with the spin axis of the satellite located in the orbital plane of the satellite and normal to the earth-sun line. Because of the drift and eccentricity of the orbit, the satellite passes through each altitude at varying local times (LT).

Data from the Air Force Geophysics Laboratory Rapid Scan Particle Detector and the NASA Goddard magnetic field monitor are used in this analysis.

The Rapid Scan Particle Detector measures fluxes of electrons and ions in the energy ranges from 100 eV to approximately 1 MeV, and from 100 eV to approximately 7 MeV, respectively. These energies are the central energies of the channels. A complete spectrum is returned for the entire energy range in each 1-s interval, but the energy resolution is low ($\Delta E/E \approx 1$).

The instrument consists of two sets of detectors. One set is mounted with the look direction oriented parallel to the spin axis, and the other set is mounted with look direction perpendicular to the spin axis. Each set of detectors consists of two cylindrical plate electrostatic analyzers (ESAs) with Spiraltron electron multipliers and two silicon surface barrier solid-state detector telescopes.

The two low- and high-energy ESAs measure the electron and ion fluxes in four contiguous channels that range from 100 eV to 1.7 keV and from 1.7 to 60 keV, respectively. Both sets of ESAs also measure a background channel with zero voltage on the deflection plate. The low-energy ESAs have geometric factors of approximately $1 \times 10^{-4} \text{cm}^2 \text{sr}$ for both ions and electrons. The high-energy ESAs have geometric factors of $3 \times 10^{-5} \text{cm}^2 \text{sr}$ for electrons and $3 \times 10^{-4} \text{cm}^2 \text{sr}$ for ions. Here we use distributions only for particles with energy greater than 20 keV.

The solid-state spectrometers (SSSs) make both anticoincident and coincident measurements. Here we use only the anticoincidence channels that measure particles between 100 and 500 keV. The electron SSSs use a 0.1-mil aluminum foil to absorb light and protons below approximately 250 keV and have a $300 - \mu\text{m}$ -thick front detector. The proton SSSs use a sweeping magnet to eliminate electrons below about 200 keV and have an approximately $6 - \mu\text{m}$ -thick front detector with 120mg/cm^2 of aluminum for a light shield. The front detectors, in anticoincidence with the rear detectors, measure the particle fluxes over the energies to be studied. A full description of the instrument and its calibration can be found in the work of Hanser, et. al. [1979].

The SCATHA magnetometer is a triaxial fluxgate magnetometer with the three sensors mounted in a mutually orthogonal configuration. The magnetometer sensors are located at the end of a 4-m boom. Each axis has a range of approximately $+500nT$ ($1nT = 10^5G$). Preflight calibration indicated that the absolute accuracy of the measurement of the ambient magnetic field along any of the three axes was better than $1nT$ at a $1 - \sigma$ confidence level. A calibration pulse built into the instrument is used to check the sensitivity levels of all three axes on orbit.

Additional information on the satellite, its configuration and material composition, and its instrumentation can be found in the work of Stevens and Vampola [1978].

3.2 SCATHA Data Analysis

Fig. 2 shows the 218 keV electron distribution functions vs L observed during the ascending portion of the satellite's orbit on April 21, 1979 (Day 111) for 40° and 90° pitch angles, along with the observed and Olson and Pfitzer [1977] model quiet magnetic field. The L value used for data presentation here, and in Figs. 4, 5, 8, and 9, is the McIlwain parameter at the position of the satellite, derived using the Olson-Pfitzer [1977] model, since this model was included in the SCATHA satellite ephemeris. As the satellite crossed $L = 6.2R_E$, there was a systematic weakening of the plasma sheet magnetic field relative to the model field, signifying the start of a magnetic disturbance. At approximately the same time (following a data gap), there was a significant dropout of 90° pitch angle electrons, producing marked butterfly distributions which characterized the sharply reduced electron fluxes out to near apogee ($L = 8R_E$). Similar effects were observed for ions at the beginning of the April 21 disturbance, but the flux dropouts recovered somewhat, and the pitch angle distributions returned to isotropic near $L = 7.4R_E$ (See ahead, Fig. 8). For the corresponding period on the previous day (the ascending portion of the orbit), which provides our baseline quiet data, no such dropouts were observed and the pitch angle distributions remained nearly isotropic over the period (See ahead, Figs. 4 and 5).

Since the particle and field variations during the ascending portion of the SCATHA orbit on 21 April 1979, are so smoothly varying and take place over a 6-hour period, we choose them for the adiabatic modeling.

To model this period, we first analyzed the magnetic field observations for the preceding quiet day. We found that a good fit (Fig. 3) to both the ascending and descending legs of the orbit is given by the Mead model if:

$$B_1 = -10nT$$

$$B_2 = 2.5nT$$

$$\phi = -3hr$$

21 APRIL 1979 (DAY III) ASCENDING

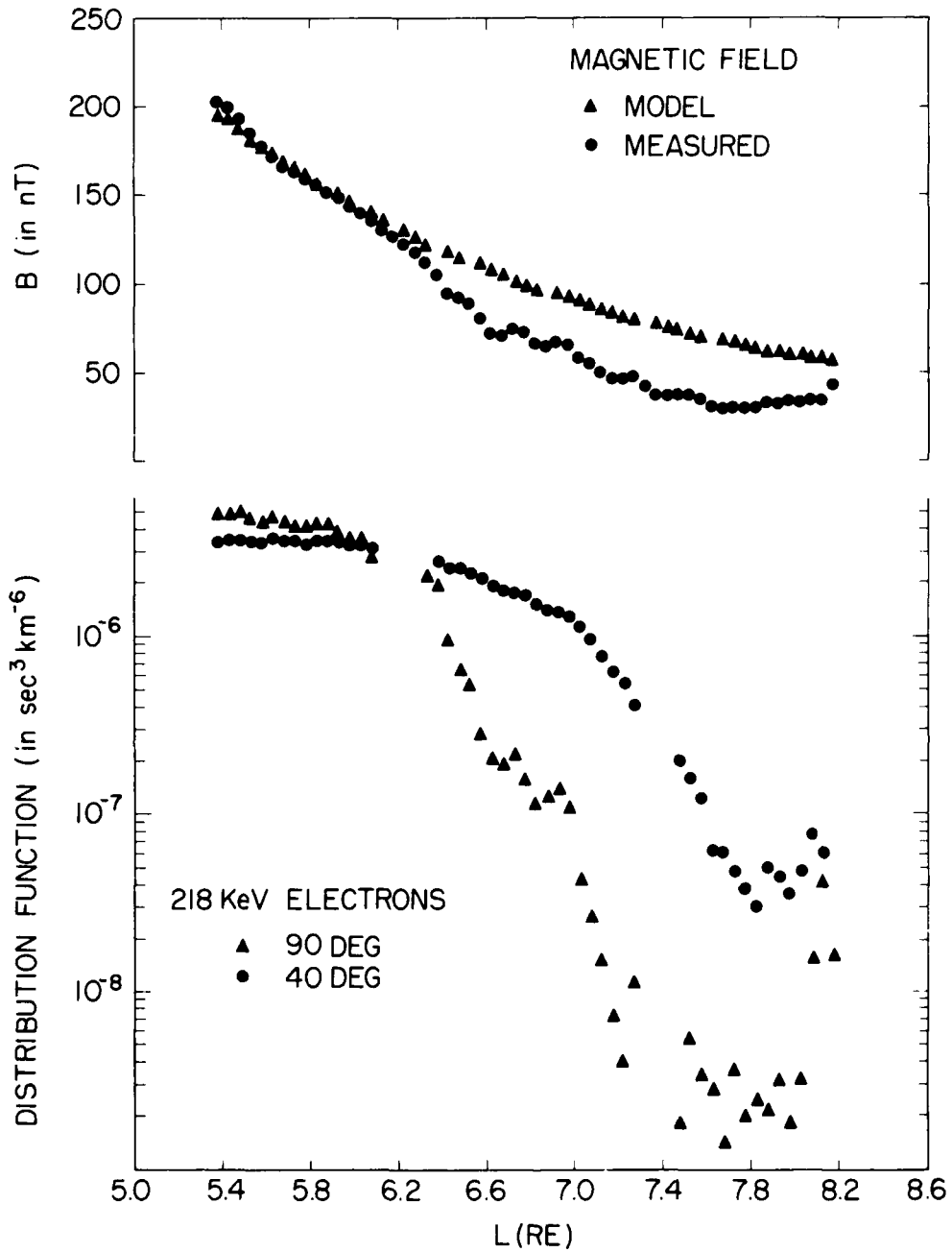


Figure 2. Top Panel: The model (Olson-Pfizer 1977) and measured magnetic fields vs. L during the ascending portion of the SCATHA orbit, 21 April 1979; Bottom panel: electron distribution function at 218keV, 40° and 90° pitch angles for the same period.

20 APRIL 1979 MAGNETIC FIELD BZ
 MEASURED (SYMBOLS) AND ADJUSTED MEAD MODEL (LINE)

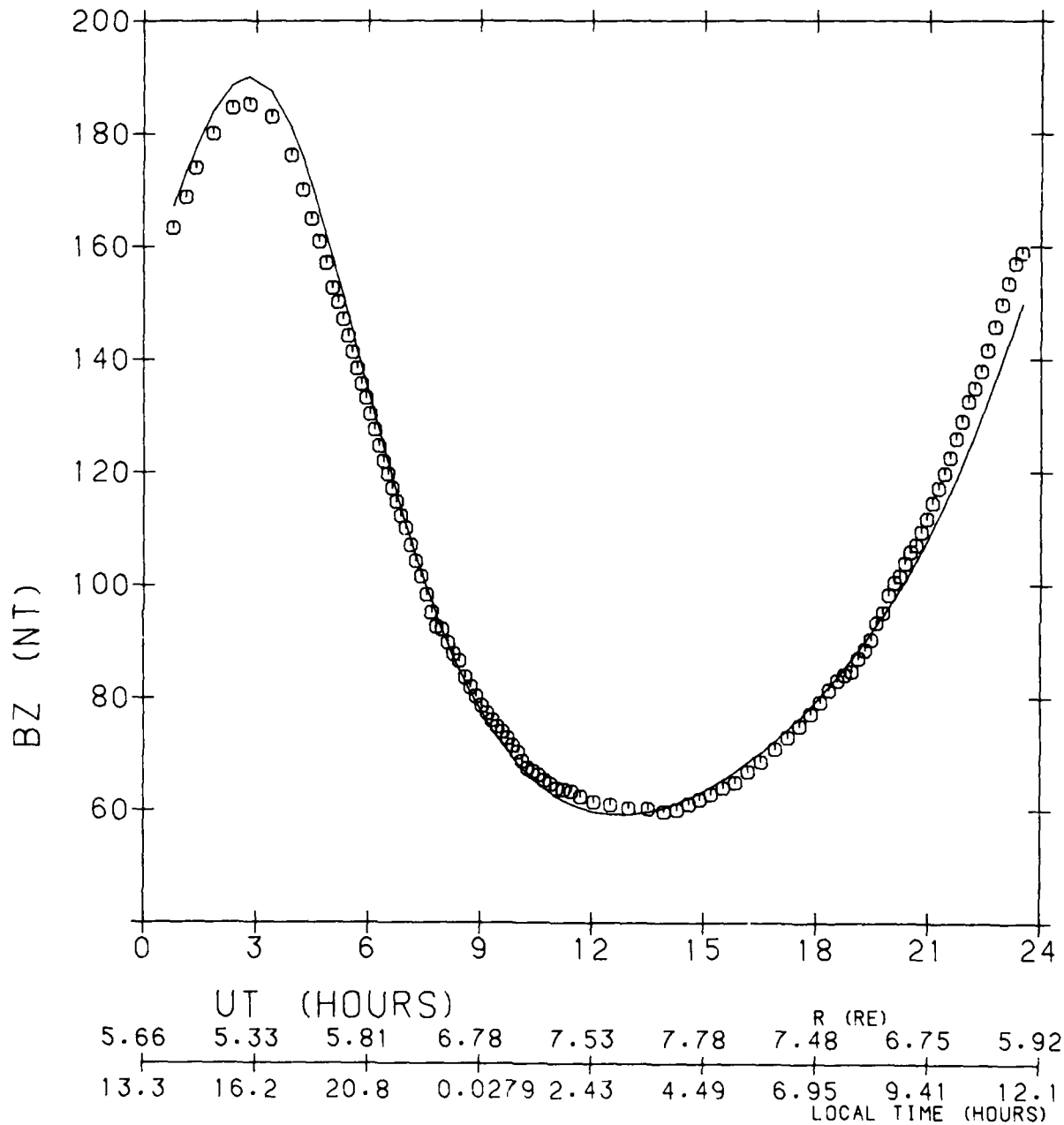


Figure 3. The magnetic field on 20 April 1979 observed by SCATHA (symbols) and computed (solid line) using an adjusted Mead model with $B_1 = -10nT$, $B_2 = 2.5nT$, $\phi = -3$ hr.

Note that it was necessary to assume a 3 hour westward rotation of the azimuthal symmetry plane in order to get a good fit to the data. Cummings, et. al., [1971] and Pfitzer, et. al. [1969], analyzing ATS-1 data, found rotations in the same direction, but only requiring 1-2 hours. The size of the rotation is attributed to the neglect of higher order multipoles in the magnetic field model in the present study, coupled with the larger radial range of the SCATHA satellite. Thus the radial variation of the neglected terms may be aliased into an apparent local time variation. The symmetric perturbation is in good agreement with that found by Mead and Fairfield [1975] for geomagnetically quiet periods. The difference between this result and the value for the original Mead [1964] model, for $10 R_E$ magnetopause distance ($-25nT$) is probably due to ring and tail currents not included in the original Mead model. Next we constructed quiet distribution functions in the form of Equation (21). For each energy channel with energy greater than 20 keV, the 90° electron and ion distribution function variations were modeled as functions of L_e , the equatorial L value computed from our model field.

Fig. 4 shows data and fits for the 275 keV ions for this period. The 90° ion distributions at noon were fit to single decaying exponentials, reflecting typical trapped ion characteristics in the outer radiation belt. High correlation coefficients were found between L_e and particle distributions for energies above 100 keV, with low correlation coefficients below, in accordance with the conventional wisdom that the magnetic field dominates control of the higher energy particles, that is, trapping them, while the lower energy particles are influenced also by electric fields. The ions characteristically displayed a steep decay, as shown here. On the other hand, the 90° electron distributions were not as well fit to single exponentially decaying functions (Fig. 5), since their variation over the same range was much less, and the shape may be influenced by the approach to the slot region between the inner and outer radiation belts.

Distribution functions mapped to noon were used to construct the weakly L -dependent anisotropy indices (from the definition in Eq. (A2) of the Appendix) found there. These are shown in Fig. 6 for the 275 keV ions and 218 keV electrons, plotted vs. the noon equatorial McIlwain L parameter obtained from our model, rather than the L parameter obtained from the Olson-Pfitzer model. Fig. 6 shows that for the ions (triangles) the pitch angle dependence at noon is strongly peaked at 90° for low L values, becoming more isotropic at larger L , that is, approaching the magnetopause. On the other hand, the electron distribution (circles) becomes more "normal" (peaked at 90°) as L increases. In both cases the variation is small.

Having constructed an L , α and energy dependent distribution function on the noon axis for the quiet period, we proceeded to model the active period magnetic field and to deduce the distributions that evolve when the adiabatic invariants are conserved.

SC5 IONS DAY NUMBER 110
 DISTRIBUTION FUNCTION (S••3/KM••6) ASCENDING

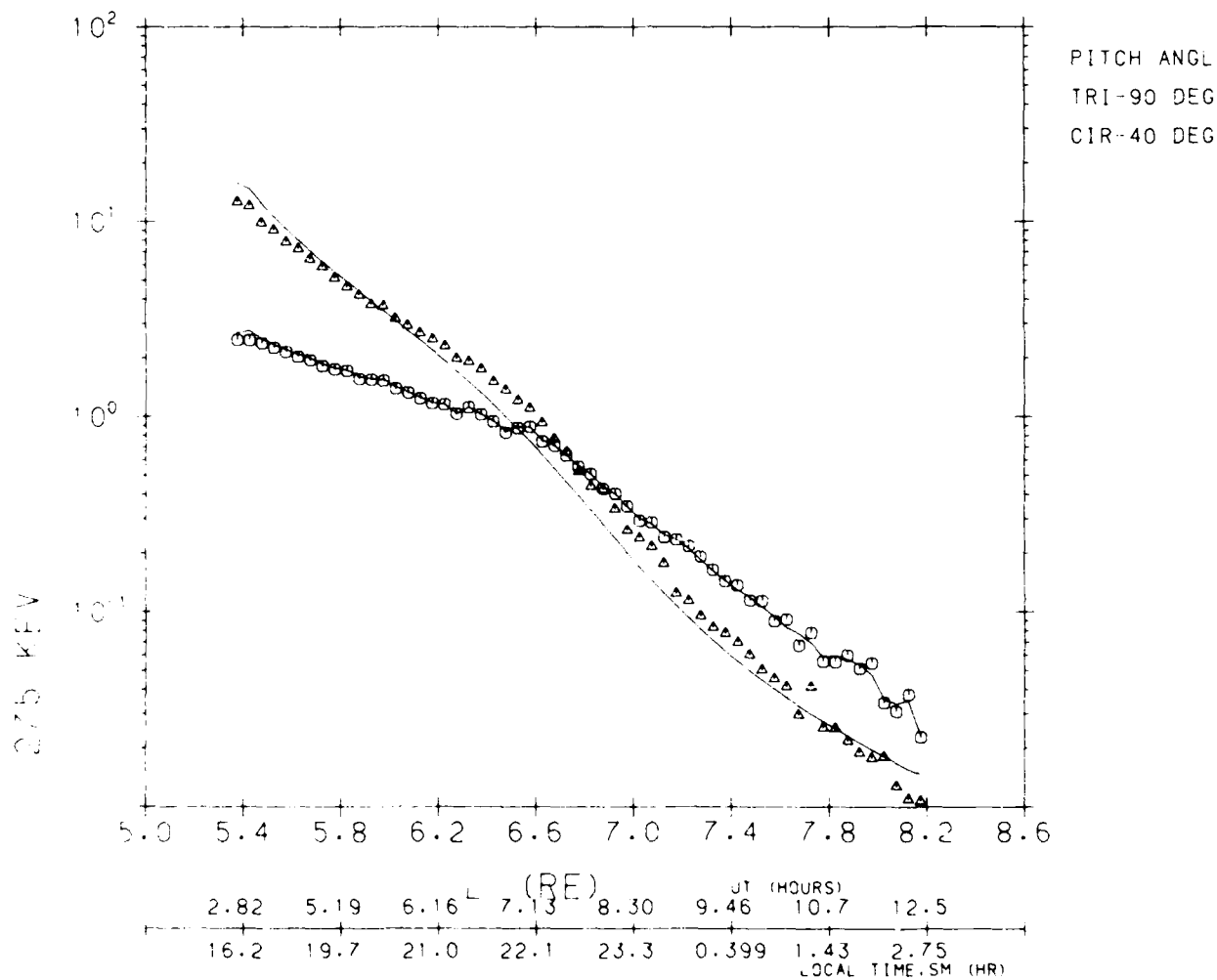


Figure 4. Comparison of measured (symbols) and fit (solid lines) distribution function values on 20 April 1979 for 275 keV ions at 40° and 90° equatorial pitch angles.

SC5 ELECTRONS DAY NUMBER 110
 DISTRIBUTION FUNCTION (S**3/KM**6) ASCENDING

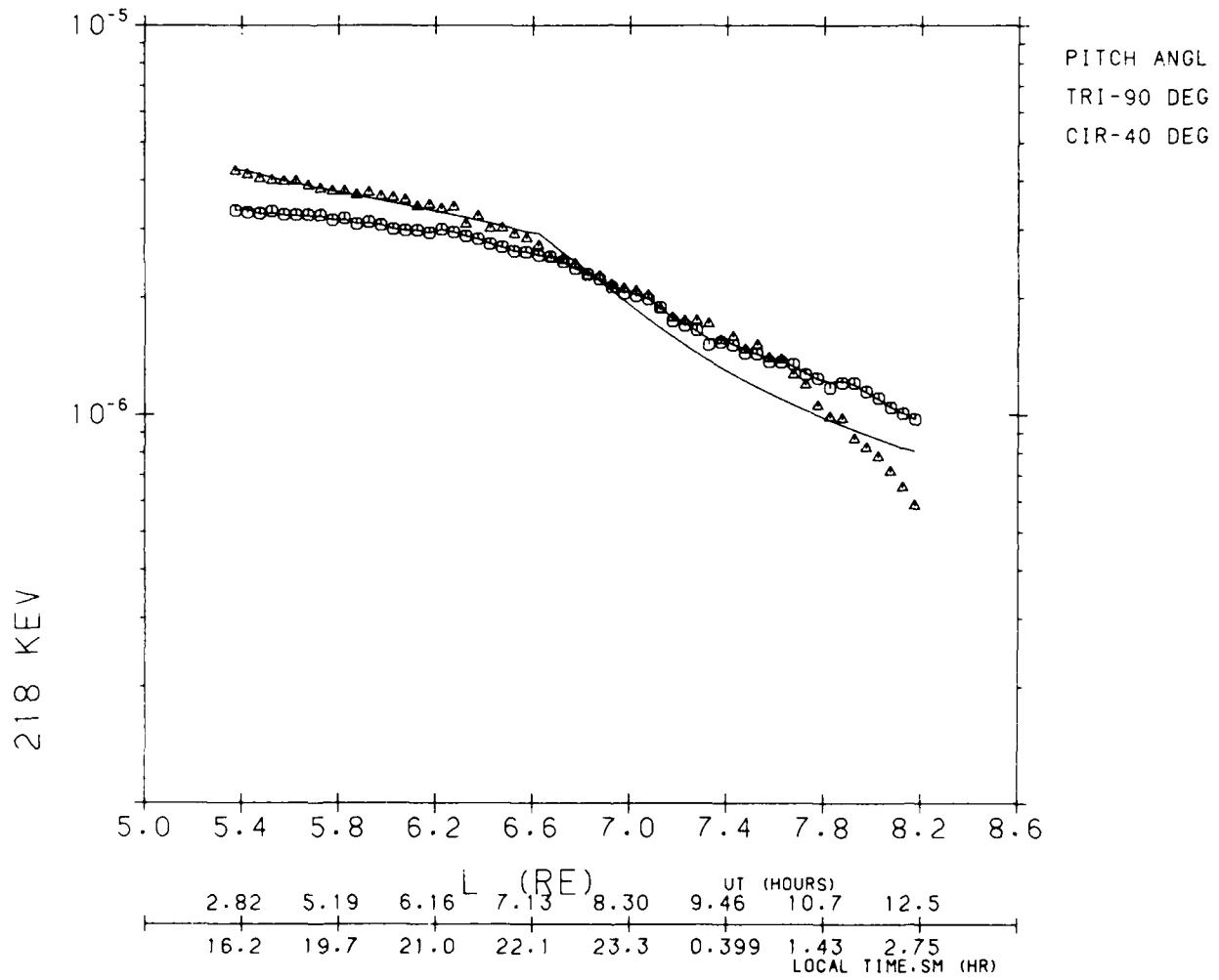


Figure 5. Same as Figure 4, but for 218 keV electrons.

SC5 NOON ANISOTROPIES DAY 110 1979

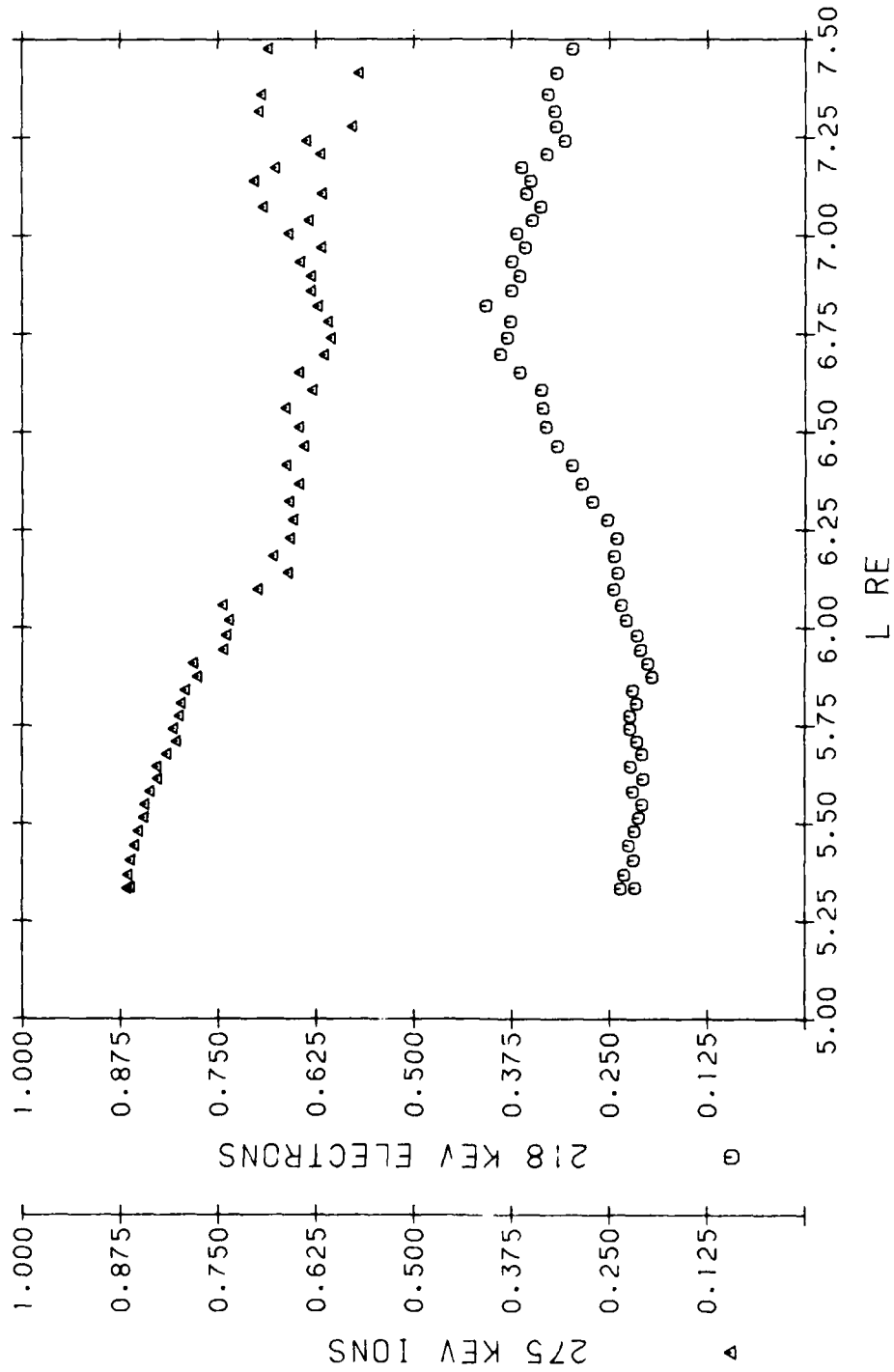


Figure 6. Noon anisotropies for 218 keV electrons (circles) and 275 keV ions (triangles) from SCATHA data, 20 April 1979.

The magnetic field for the disturbed period (Fig. 7) was modeled in such a way that the asymmetric contribution, defined by the parameters B_2 and ϕ according to Eq. (7), remained the same throughout. This contribution resulted in a more tail-like field than for the previous quiet day, stretched on the night side, and compressed on the day side. The symmetric contribution, as defined by B_1 , was allowed to vary with time, to simulate the rapid (approximately 2-hour) decompression found in the data. The final field is thus decompressed and tail-like, relative to the field used for the previous quiet day.

Fig. 8 gives the predicted values (solid lines) for the 275 keV ion distribution function at 90° and 40° for the disturbed period, as well as the measured values, both along the SCATHA orbit. The two show excellent agreement both before and during the initial phase of the disturbance, up to L of $7 R_E$. Recall that at this point the model field reached its most tail-like and decompressed configuration, and is unchanging hereafter (Fig. 7). Beyond $L = 7$, the 40° pitch angle prediction agreement continues through L approximately 8, but a 90° source at high L is apparent. Fig. 9 is a similar plot for the 218 keV electrons. The agreement is not nearly as good, although the butterfly distribution characterizing the disturbance is reproduced as for the ions at the onset of the field variation. The electron dropout is much greater than adiabatic variations predict during decompression, and may indicate their greater interaction with waves. It is expected that the results would be similar for other energies above 100 keV, but these have not been included due to lack of resolution and reliable observation over a sufficiently large energy range. More specifically, to calculate the distribution functions for a specific set of variables in the disturbed field, it is necessary to have seen these particles, with a different set of variables, in the reference field. For this particular exercise, we need to use observations in the reference field at higher energies, up to a factor of 2 from those for which we are predicting. The reliable upper limits for the SCATHA detector we used were 335 keV for electrons and 1 MeV for the ions.

4. DISCUSSION

In this complex exercise, we have demonstrated that when relatively slow variations of the magnetospheric magnetic field occur, changing distribution functions, calculated from the three adiabatic invariants in a relatively simple time-varying magnetic field model, can be used to evaluate real particle sources and losses in the geosynchronous regime. The method applies only to particles whose energies are sufficiently high that electric field effects can be assumed negligible.

In the case treated here we found that, coincident with a factor of 2 decompression in the magnetic field, we have observed a factor of 100 depletion of 90° equatorial pitch angle high energy trapped electrons in the outer radiation belt and a factor of 10 depletion of 90° equatorial pitch angle high energy trapped ions. Substantially smaller depletions were found for lower pitch angles, thus resulting in the appearance of marked butterfly pitch angle distributions. The predicted adiabatic variations

DAY 111 MEAD PARAMETERS

B2 = 6.4 NT PHI = -2 HR

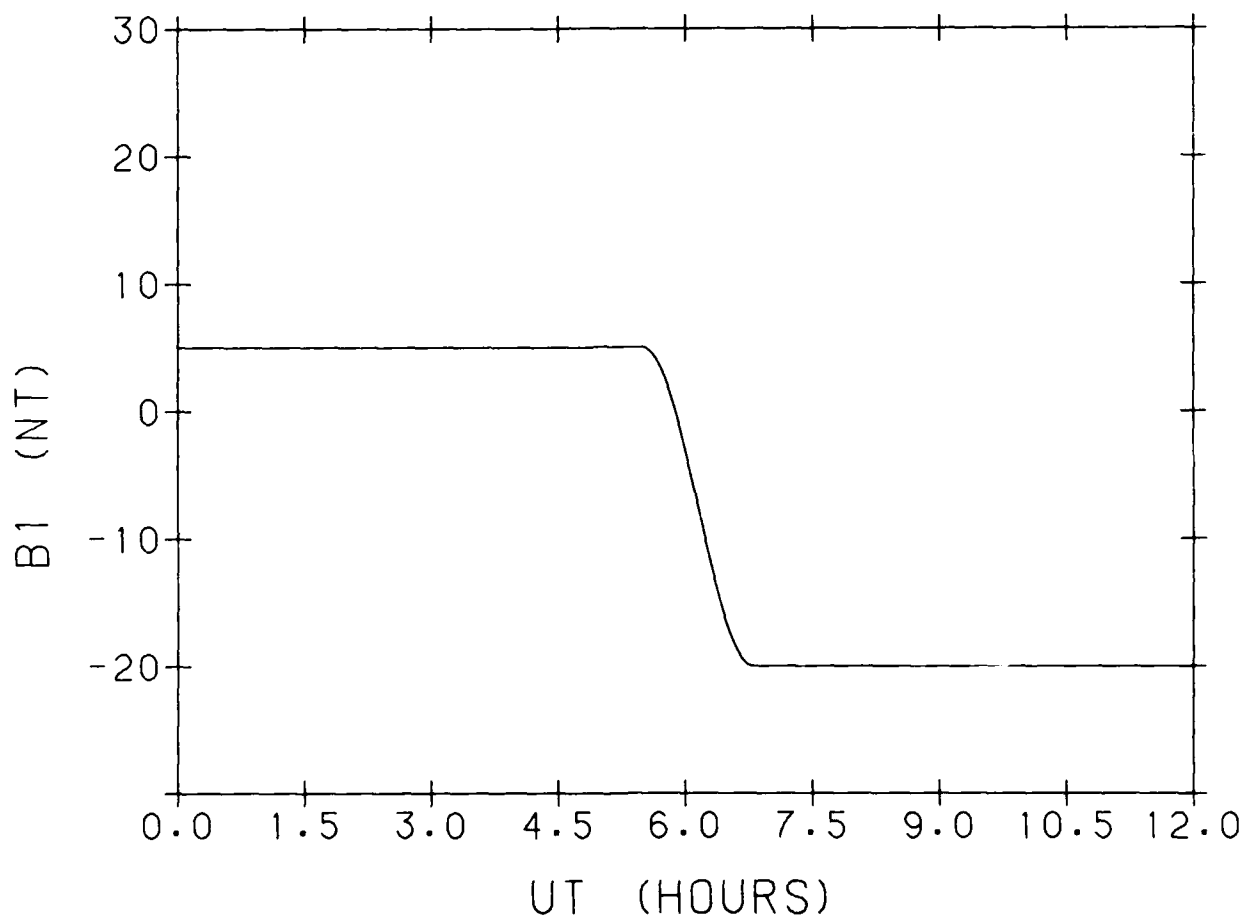


Figure 7. Adjusted Mead model magnetic field parameters for 21 April 1979.

SC5 IONS DAY NUMBER 111
 DISTRIBUTION FUNCTION (S••3/KM••6) ASCENDING

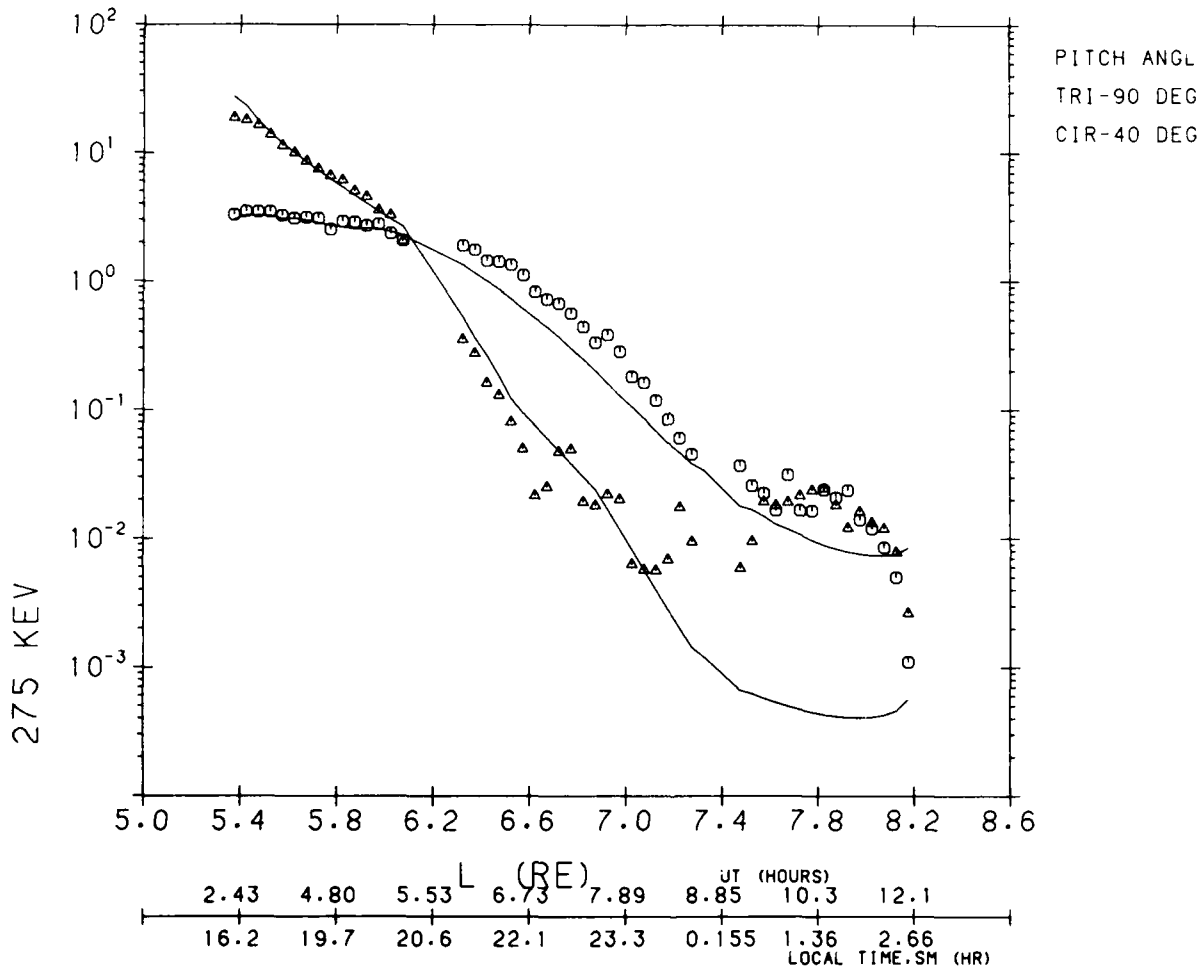


Figure 8. Comparison of SCATHA observations (symbols) of 275 keV ions on 21 April 1979 with predictions (solid lines) based on adiabatic variations from the previous day.

SC5 ELECTRONS DAY NUMBER 111
 DISTRIBUTION FUNCTION (S••3/KM••6) ASCENDING

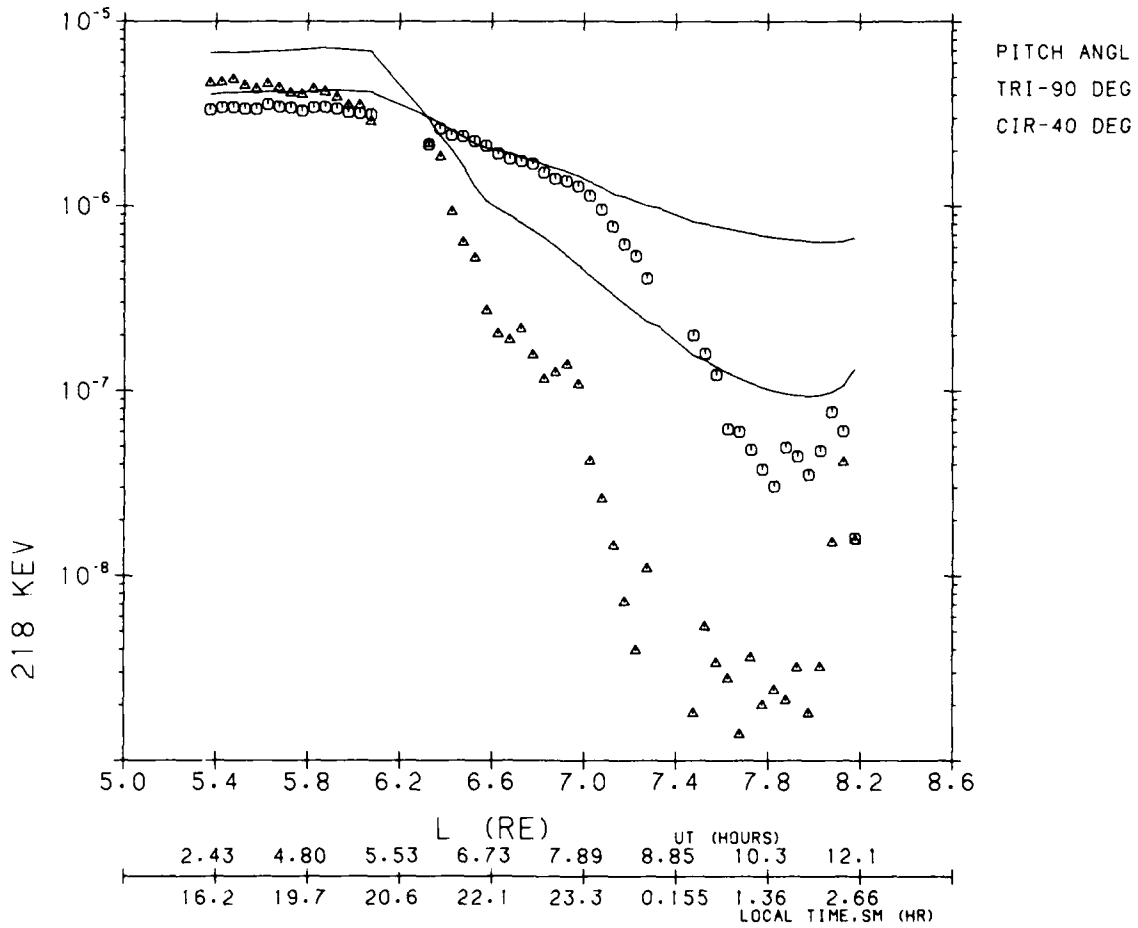


Figure 9. Same as Figure 8, but for 218 keV electrons.

are factor of 10 depletions of both 90° electrons and ions and relatively little changes in the 40° particles. These variations are in very good agreement with those observed for the ions, except for the observed increases at high L ; in particular, the butterfly pitch angle distribution is reproduced. Substantially greater losses are observed for the electrons than predicted for the entire radial range covered during the magnetic decompression, but, as for the ions, the butterfly pitch angle distribution is reproduced.

Limitations of our procedure include the use of a very simple magnetic model. The Mead mathematical form was chosen as a tradeoff between speed and accuracy. In analyzing the large amount of data expected from a mission such as CRRES, a computationally simple technique is essential. The Mead model did result in a possibly unrealistically large rotation of the azimuthal symmetry plane, which needs to be examined against other quiet model predictions. The weakness of the model is most significant at large radial distances, where both the adiabatic approximation and the first-order drift shell perturbation method would be expected to break down, anyhow (both spatial and temporal variations are large relative to a zeroth order dipole field). For the example studied here, we note that at large L , the ions and electrons behave differently with respect to the adiabatic predictions (the ion population increases, while the electron population decreases), thus indicating real sources and sinks as the origin of disagreement, rather than simplicity in the magnetic field model. An additional limitation in the present study is in the energy range and resolution of the available data. Since the adiabatic theory predicts changes in particle energy in response to changes in the magnetic field, specification of the quiet distribution functions over extended energies and radial positions is required to estimate the adiabatic change in the distributions observed in a particular energy channel. The particular energy channels depicted in this study were chosen because the data coverage in their immediate energy neighborhoods was the best on the SCATHA satellite. The results are not expected to be different for higher energies, for any reasonable energy distribution (exponential falloff with increasing energies), since the magnetic decompression would produce a deceleration of adiabatically responding particles, so that those observed in a given energy channel during the decompression were in a higher energy channel before.

Thus we conclude that adiabatic responses of trapped particle distributions can be large (order of magnitude), and that such responses can be mechanisms for production of butterfly pitch angle distributions. It therefore appears that pitch angle distributions of selected classes of geomagnetically trapped particles could serve as indicators of magnetic disturbances, and could therefore serve as valuable aids in analysis of trapped particle data, such as that expected from the forthcoming CRRES mission; the pitch angle distribution of a selected particle could be used to estimate a magnetic parameter using the reverse of the procedure followed here.

REFERENCES

- Chapman, S. and Bartels, J., *Geomagnetism*, Oxford University Press, London, 1940.
- Cummings, W. D., Coleman, P. J., Jr., and Siscoe, G. L., "Quiet day magnetic field at ATS-1", *J. Geophys. Res.*, Vol. 76, No. 4, Pp. 926-932, 1971.
- Frank, I. A., "On the extraterrestrial ring current during geomagnetic storms", *J. Geophys. Res.*, Vol. 72, No. 15, Pp. 3753-3767, 1967.
- Hanser, F. A., Hardy, D. A., and Sellers, B., *Calibration of the Rapid Scan Particle Detector Mounted in the SCATHA Satellite*, Tech. Report, AFGL-TR-79-0167, ADA082382, Air Force Geophysics Laboratory, Hanscom AFB, MA, 1979.
- Kaye, S. M., Lin, C. S., Parks, G. K., and Winckler, J. R., "Adiabatic modulation of equatorial pitch angle anisotropy", *J. Geophys. Res.*, Vol. 83, No. A6, Pp. 2675-2682, 1978.
- Lin, C. S., Parks, G. K., and Winckler, J. R., "The 2- to 12-min quasi-periodic variation of 50- to 1000-keV trapped electron fluxes", *J. Geophys. Res.*, Vol. 81, No. 25, Pp. 4517-4523, 1976.
- Luhmann, J. G., and Schulz, M., "Magnetic shell tracing: A simplified approach", p. 582 in *Quantitative Modeling of Magnetospheric Processes*, W. P. Olson, Ed., American Geophysical Union, Washington, 1979.
- Lui, A. T. Y., McEntire, R. W., and Krimigis, S. M., "Evolution of the ring current during two geomagnetic storms", *J. Geophys. Res.*, Vol. 92, No. A7, Pp. 7459-7470, 1987.
- Lyons, L. R., and Williams, D. J., "Storm-associated variations of equatorially mirroring ring current protons, 1-800 keV, at constant first adiabatic invariant", *J. Geophys. Res.*, Vol. 81, No. 1, Pp. 216-220, 1976.
- Lyons, L. R., "Adiabatic evolution of trapped particle pitch angle distributions during a storm main phase", *J. Geophys. Res.*, Vol. 82, No. 16, Pp. 2428-2432, 1977.
- McIlwain, C. E., "Coordinates for mapping the distribution of magnetically trapped particles", *J. Geophys. Res.*, Vol. 66, No. 11, Pp. 3681-3691, 1961.
- Mead, G. D., "Deformation of the geomagnetic field by the solar wind", *J. Geophys. Res.*, Vol. 69, Pp. 1181-1195, 1964.

References (cont'd)

Mead, G. D., and Fairfield, D. H., "A quantitative magnetospheric model derived from spacecraft magnetometer data", *J. Geophys. Res.*, Vol. 80, No. 4, Pp. 523-534, 1975.

Olson, W. P., and Pfitzer, K. A., "A quantitative model of the magnetospheric magnetic field", *J. Geophys. Res.*, Vol. 79, No. 25, Pp. 3739-3748, 1974.

Olson, W. P., and Pfitzer, K. A., *Magnetospheric Magnetic Field Modeling, Annual Scientific Report*, AFOSR Contract No. F44620-75-C-0033, McDonnell Douglas Astronautics Company- West, Huntington Beach, CA, 1977.

Paulikas, G. A., and Blake, J. B., "Effects of sudden commencements on solar protons at the synchronous orbit", *J. Geophys. Res.*, Vol. 75, P. 734, 1970.

Pennington, R. H., "Equation of a charged particle shell in a perturbed dipole field", *J. Geophys. Res.*, Vol. 66, No. 3, Pp. 709-712, 1961.

Pfitzer, K. A., Lezniak, T. W., and Winckler, J. R., "Experimental verification of drift-shell splitting in the distorted magnetosphere", *J. Geophys. Res.*, Vol. 74, No. 19, Pp. 4687-4693, 1969.

Roberts, C. S., "Pitch-angle diffusion of electrons in the magnetosphere", *Rev. Geophys.*, Vol. 7, P. 305, 1969.

Schulz, M., and Boucher, D. J., Jr., "Orthogonal basis functions for pitch angle diffusion theory", Pp. 159-168 in *Physics of Space Plasmas (1982-4)*, J. Belcher, H. Bridge, T. Chang, B. Coppi, and J. R. Jasperse, Ed., Scientific Publ., Inc., Cambridge, MA, 1984.

Schulz, M., and Lanzerotti, L. J., *Particle Diffusion in the Radiation Belts*, Springer-Verlag, Berlin/ Heidelberg/New York, 1974.

Soraas, F., and Davis, L. R., *Temporal Variations of the 100 keV to 1700 keV Trapped Protons Observed on Satellite Explorer 26 During the First Half of 1965*, GSFC X-612-68-328, NASA, Greenbelt, MD, 1968.

Stern, D., "Classification of magnetic shells", *J. Geophys. Res.*, Vol. 70, No. 15, Pp. 3629-3634, 1965.

Stern, D., "Euler potentials and geomagnetic drift shells", *J. Geophys. Res.*, Vol. 73, No. 13, Pp. 4373-4378, 1968.

References (cont'd)

Stevens, J. R., and Vampola, A. L., (eds), *Description of the Space Test Program P78-2 Spacecraft and Payload*, Rep. SAMSO TR-78-24, Air Force Systems Command, Los Angeles, CA., 1978.

Tsyganenko, N. A., and Usmanov, A. V., "Determination of the magnetospheric current system parameters and development of experimental geomagnetic field models based on data from IMP and HEOS satellites", *Planet. Space Sci.*, Vol. 30, No. 10, Pp. 985-998, 1982.

Walt, M., *Loss Rates of Trapped Electrons by Atmospheric Collisions*, p. 337 in *Radiation Trapped in the Earth's Magnetic Field*, B. M. McCormac, ed., D. Reidel, Dordrecht, Holland, 1966.

Williams, D. J., Arens, J. F., and Lanzerotti, L. J., "Observations of trapped electrons at low and high altitudes", *J. Geophys. Res.*, Vol. 73, P. 5673, 1968.

APPENDIX

We discuss what happens to a group of electrons in a dipole field initially distributed uniformly in a circular ring of inner radius $6.5R_E$ and outer radius $7R_E$. After the field is slowly (such that the adiabatic approximations apply) distorted into a Mead field, compressed at the dayside and tail-like on the nightside, we will see strong pitch angle dependence in the way a typical magnetic perturbation affects the particle trajectories and energies. Particles closest to 90° equatorial pitch angle suffer the greatest changes in drift orbit and energy.

The initial distribution function, F , for the electrons in the dipole field is given by:

$$\frac{F}{c^3} = F_0 \sin \alpha \text{ for } 6.5 \leq L \leq 7R_E;$$

$$\frac{F}{c^3} = 0 \text{ for } L < 6.5R_E \text{ and } L > 7R_E. \quad (A1)$$

Here α is the pitch angle. F_0 is nominally taken as $1km^{-3} keV^{-3}$ in the energy interval 300-400 keV, and zero for other energies.

For later comparison we list in Table A1 the values of selected parameters for the initial distribution. They are, of course, constant in azimuth and L between 6.5 and $7R_E$. The average energy is the ratio of the energy density (second moment of the distribution function) to the number density (zeroth moment). Using the values of the distribution functions at pitch angles of 45° and 90° , the anisotropy index is defined as:

$$A = 1 - \frac{F(\alpha = 45^\circ)}{F(\alpha = 90^\circ)}. \quad (A2)$$

Distributions peaked strongly at 90° will have anisotropy close to 1; distributions strongly peaked at 45° (butterfly) will have negative anisotropy.

The distorted or perturbed field is a Mead field with the following parameters:

$$\bar{g}_1^0 = -B_1 = 10nT;$$

$$\bar{g}_2^1 = \frac{B_2}{\sqrt{3}} = 2nT;$$

$$\phi = 0.$$

Between 6.5 and 7 R_E the dipole field falls from 113 to 90 nT in the equatorial plane. In the same radial interval the Mead field we are using has values at noon of 144-124 nT , a compression of 27-38 percent. At midnight the values are between 102 and 76 nT , a weakening of the field by 10-15 percent.

When the initial distribution is adiabatically rearranged by the new field, the parameters in Table A1 have the two-dimensional structures seen in Figures A1 and A2. In these calculations the energy integration is done analytically, and the pitch angle integration is done by summing over 10° bins. Figure A1 shows equatorial maps of the omnidirectional (top panel), 90° pitch angle (middle panel), and 40° pitch angle (bottom panel) energy densities and average energies in the left-hand columns and right-hand columns, respectively. The omnidirectional displays in the top panel illustrate the large radial spread at local noon, relative to the initial configuration, and the deceleration of the electrons (recall that the average energy in the dipole field was 350 keV). The 90° pitch angle electrons suffer the most distortion in their drift orbits, and the most energy loss, as seen by comparing the bottom two panels of the figure. The drift orbit distortion produces the radial spread at local noon seen in the top panel. The local time asymmetry in the energy density of the 40° electrons, shown in the bottom panel, illustrates the local time dependence of the pitch angle shift caused by the perturbation. The particles seen at local noon at 40° pitch angle in the perturbed field had lower pitch angles in the dipole field than those particles seen at local midnight at 40° pitch angle in the perturbed field. Figure A2, which maps the pitch angle anisotropy (-1 for extreme butterfly distribution, +1 for extreme normal distribution), illustrates the almost complete separation of 90° and 40° particles at noon and midnight. At noon the higher pitch angle electrons are confined to the outer radii, and the lower pitch angle electrons are confined to the inner radii, while the reverse is true at midnight.

Table A1. Parametric Values for Initial Electron Distribution

Distribution	
Energy Density (Omnidirectional)	$2.1 \times 10^{11} keV/km^3$
Average Energy (Omnidirectional)	350keV
Energy Density (Unidirectional at 90°)	$2.1 \times 10^{10} keV/km^3/sr$
Average Density (Unidirectional at 90°)	350keV
Energy Density (Unidirectional at 40°)	$1.3 \times 10^{10} keV/km^3/sr$
Average Density (Unidirectional at 40°)	350keV
Anisotropy	0.293

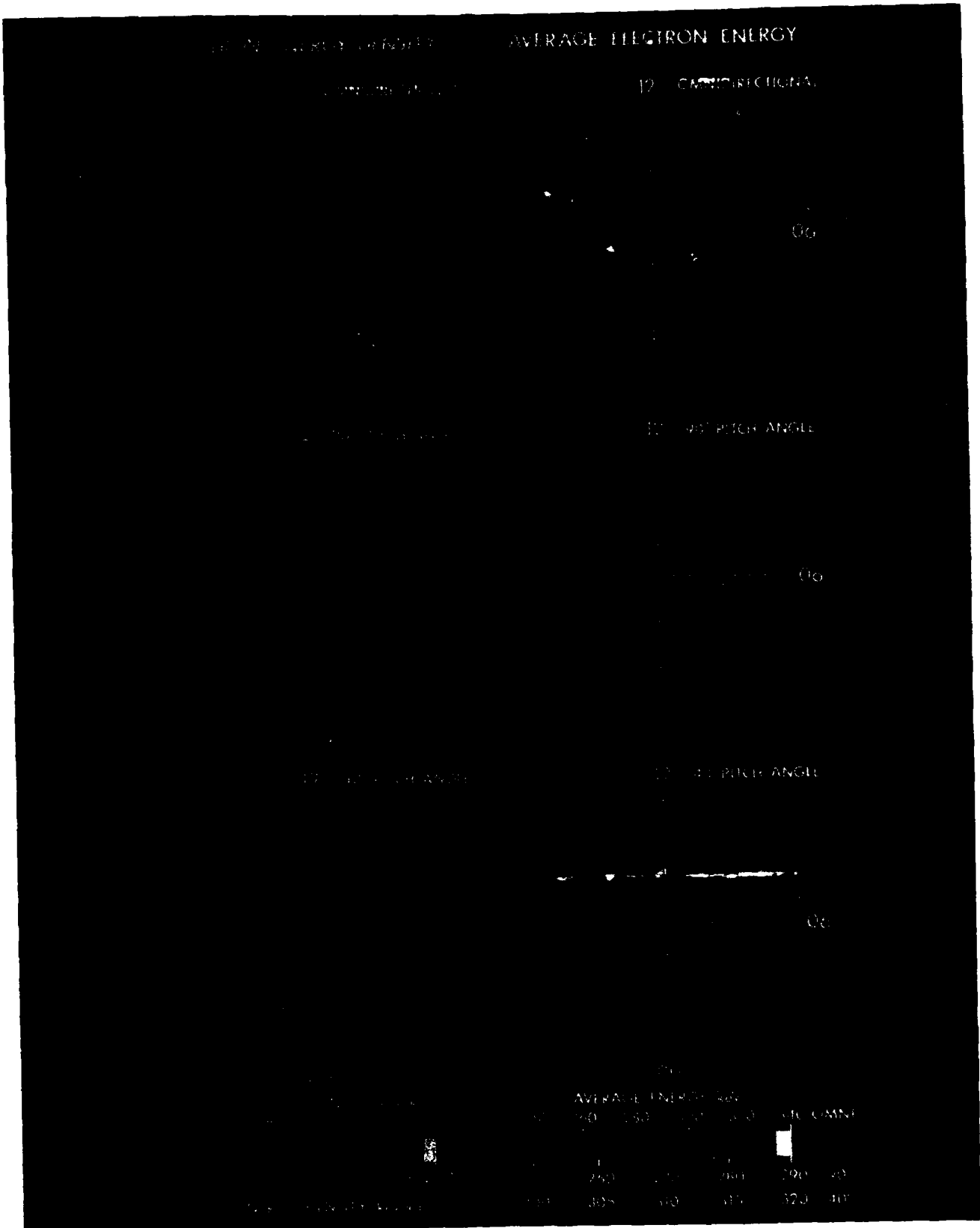


Figure A1. Equatorial maps of energy density (left-hand column) and average energy (right-hand column) in a Mead field with $B_1 = -10nT$, $B_2 = 3.4nT$, and $\phi = 0$, deduced by adiabatic variation for electrons initially in a dipole field and initially distributed uniformly between 300 and 400 keV and between 6.5 and $7.0R_E$, with a $\sin \alpha_e$ equatorial pitch angle distribution. The omnidirectional maps are shown in the top panel; the maps for the 90° pitch angle electrons in the middle panel; and the maps for the 40° pitch angle electrons in the bottom panel.

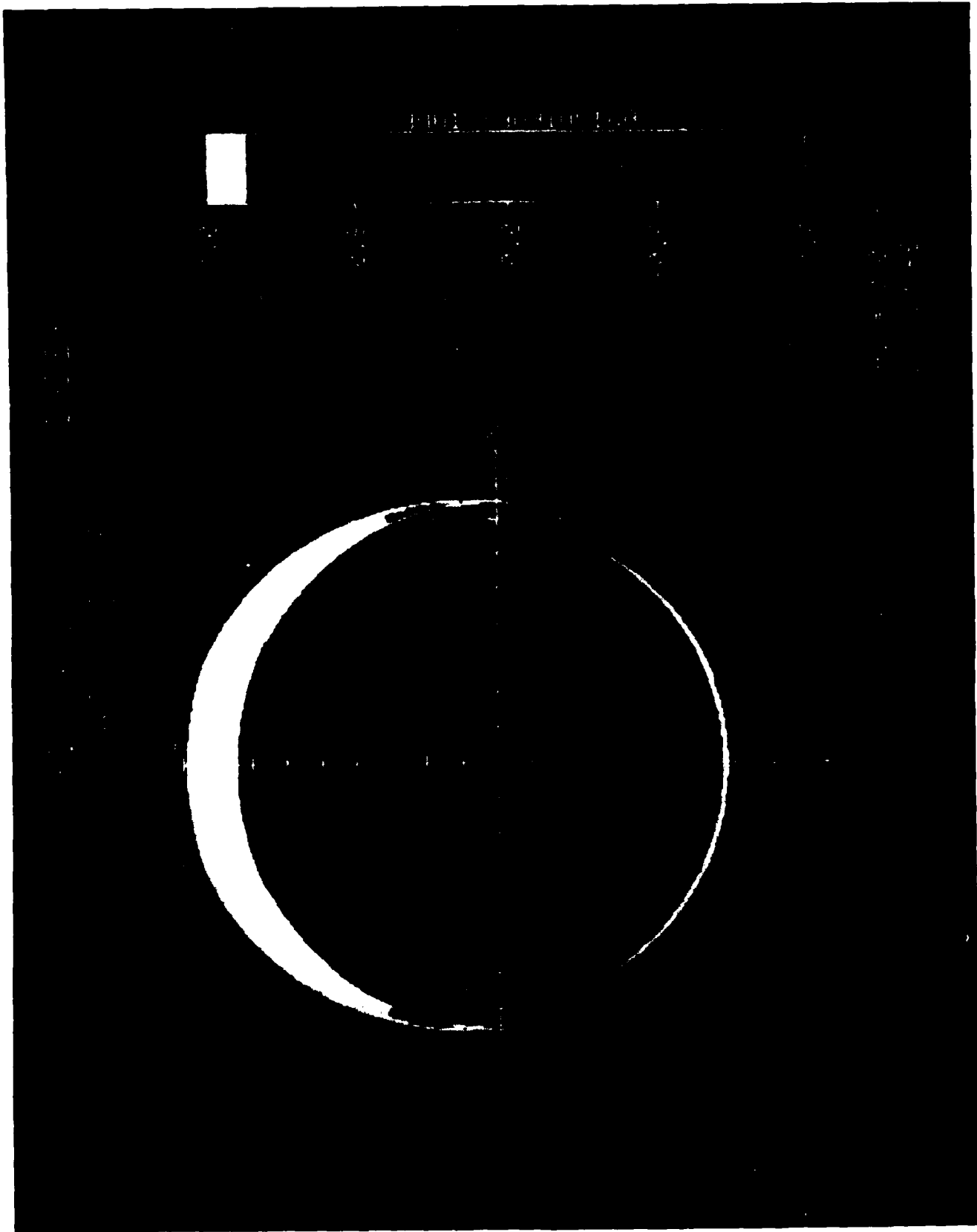


Figure A2. Anisotropy index for 270 keV electrons in the same Mead field as in Figure A1, deduced by adiabatic variation for electrons with the same initial distribution in a dipole field as in Figure A1.